CHAPTER 2

Experimental techniques and theoretical background

2.1. Introduction

This chapter gives an overview of the various experimental techniques employed for characterizing the different liquid crystalline compounds and mixtures. Related principle of operation and working of the setups have been described in brief. In addition, a few molecular theories, describing the behavior of different liquid crystalline phases and related to the subject matter of the present dissertation, have also been portrayed in a nutshell.

2.2. Experimental techniques

2.2.1. Texture study

Analysis of textures by Polarizing Optical Microscopy (POM) is one of the essential techniques for preliminary identification of different liquid crystalline phases and for resolving the related phase transition temperatures. When a mesogenic sample is examined under a polarized light, a wide variety of characteristic patterns, known as textures, are observed. The formation of such textures is principally decided by the defect structure occurring in the long range molecular order in the liquid crystalline medium. A careful inspection of such textures and the temperature dependant variation of them can enable one to extract valuable information regarding their phase-structure and related transition schemes.

The samples under study were introduced between a glass slide and a cover slip and placed in a hot stage Mettler Toledo FP-82 HT equipped with the Mettler Toledo FP 90 central processing system. The textures were observed with the aid of a polarizing optical microscope – Motic BA300 with Moticam 580 (5.0 MP) CCD camera attachment. From the precise study of temperature dependencies of textures and related topology of defects, the different mesophases were assigned and transition temperatures were also recorded. A comprehensive account of various textures along with photographs has been presented by Demus *et al.* [1] and Dierking [2].

2.2.2. Differential Scanning Calorimetry

Differential Scanning Calorimetry (DSC) is a thermal technique that plays an important role in characterizing new liquid crystalline phases and serves as a complementary process to polarizing optical microscopy and X-ray diffraction study. By assessing the enthalpy change coupled with a transition, DSC is capable of identifying the nature of phase transition [3–5]. It also helps in extracting other valuable information regarding conformational disorder [6], purity of the sample [7] and so on. However, DSC is not suitable for isolating those transitions where the associated enthalpy changes are relatively less.

In this work, determination of phase transition temperatures and transition enthalpies of a few hockey stick-shaped liquid crystals were carried out with the help of a Perkin Elmer Pyris 1 Differential Scanning Calorimeter at the Institute of Chemistry–Physical Chemistry, Martin-Luther-University Halle-Wittenberg, Halle (Saale), Germany.

2.2.3. X-ray diffraction study

The structural analysis of liquid crystalline compounds and study of related molecular properties on a quantitative basis can conveniently be carried out with the aid of X-ray diffraction studies. Regarding such measurements in

liquid crystalline materials, a number of exhaustive reviews are available [8–13].

The theoretical interpretation of outcomes from X-ray diffraction measurements in mesogenic compounds was put forwarded by Vainstein [14] and Leadbetter [15, 16]. From an analysis of the X-ray diffraction pattern, the Fourier image of the correlation density function could be obtained. The reconstruction of the same from the scattered X-ray data provides knowledge on both the relative organization of molecules and specific characteristics of the orientational and translational order in a mesogen.

The nature of the X-ray diffraction pattern of a liquid crystalline material can conveniently be explained by considering the director distribution or ordering of the molecules within the medium. The pattern of an unoriented nematic sample consists of a uniform halo just like that of an isotropic liquid. This is due to the fact that in general, a nematic liquid crystal encompasses a large number of domains, within each of which the molecules are oriented along a specific direction, i.e., along the director $\hat{n}$, but there is no such preferential alignment of the sample as a whole so that the diffraction pattern possesses symmetry of revolution around the direction of the incident X-ray beam. However, application of a suitable external perturbing field – magnetic or electric – of appropriate strength or a surface alignment can cause a ‘monodomain’ or ‘aligned’ or ‘oriented’ specimen of liquid crystal. The schematic presentation of small angle X-ray diffraction pattern for a nematic liquid crystal oriented perpendicular to the direction of the incident X-ray beam is illustrated in the figure 2.1(a). Here, the principal halo splits into two crescents, having maximum intensity along the equatorial direction, i.e., perpendicular to the director. These crescents are formed primarily due to intermolecular scattering. Related Bragg angle provides a measure of the lateral intermolecular distance. Furthermore, in the meridional direction (parallel to the director) two more crescents are observed at a much smaller angle and the corresponding Bragg angle is a measure of the apparent molecular length. In

some cases, the inner diffuse crescents are found to be replaced by sharp spots [figure 2.1(b)], i.e., the intensity of small angle scattering is much stronger than that of the wide angle scattering and the corresponding phase is termed as the 'cybotactic nematic phase'. The presence of the sharp spots indicates the existence of domains or clusters with smectic like layered structure in the nematic phase, which are designated as 'cybotactic' groups [17, 18].

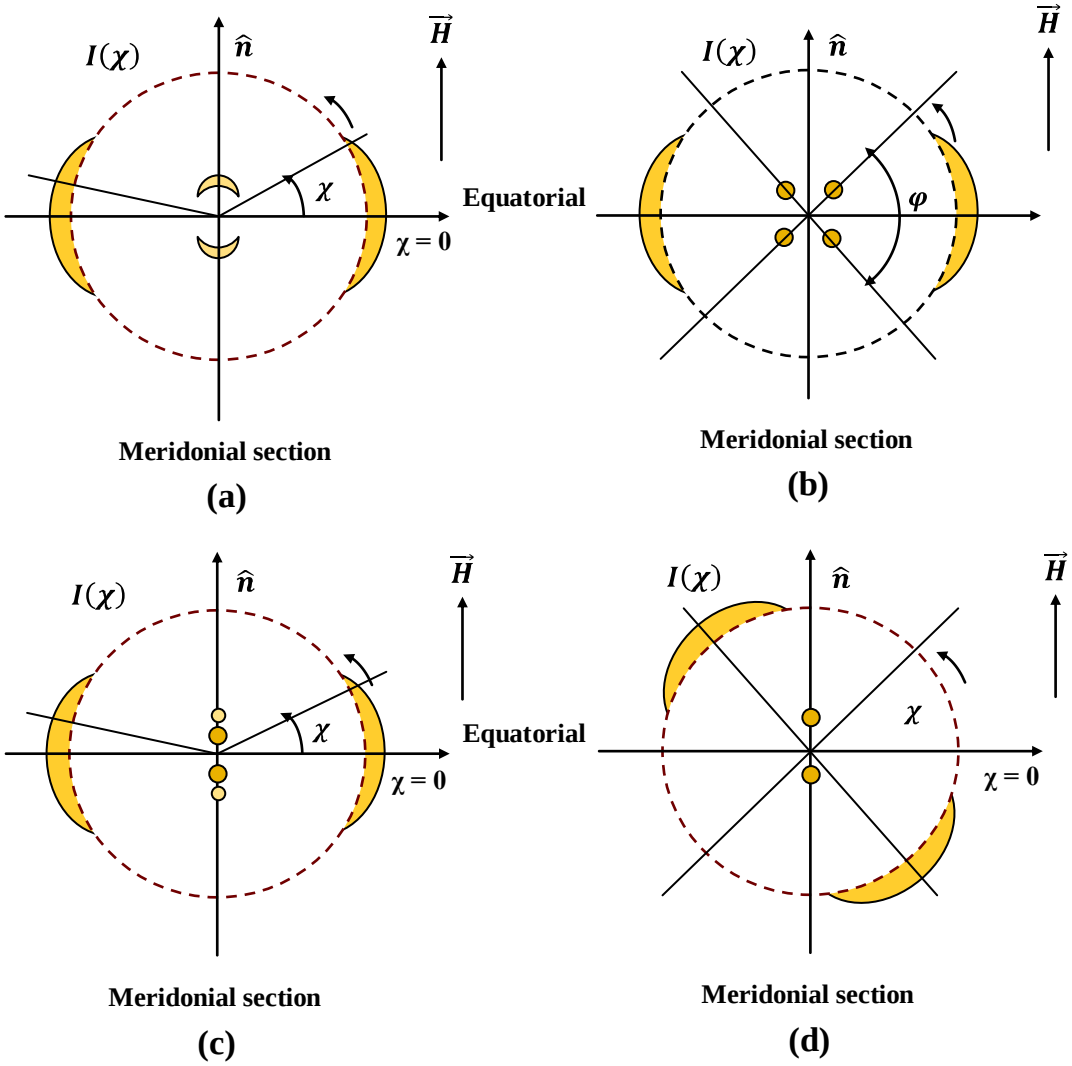

FIGURE 2.1. Schematic representation of X-ray diffraction pattern of an oriented **(a)** nematic, **(b)** skewed cybotactic nematic, **(c)** smectic *A* and **(d)** smectic *C* liquid crystal.

The X-ray diffraction pattern of smectic *A* (Sm-*A*) phase is shown in figure 2.1(c). Since Sm-*A* phase can have only quasi-long range order along its

layer normal [19, 20], the second order Bragg reflections in the meridional direction are generally very weak and are often absent in the X-ray photographs. The meridional spots are formed due to Bragg reflection from the layers and are analyzed to determine the layer thickness (*d*).

Figure 2.1(d) gives the schematic representation of X-ray diffraction pattern in the smectic *C* (Sm-*C*) phase with tilted molecular arrangement, where the incident X-ray beam is parallel to the layer normal. As there is no azimuthal preference for molecular tilt in the Sm-*C* phase, the tilting may occur in dissimilar azimuthal orientations.

An inspection of the X-ray diffraction pattern of aligned samples, yields the angular distribution of the X-ray intensity in the outer diffraction arc [i.e., X-ray intensity $I(\chi)$ *vs.* azimuthal angle (χ) curve], which can be analyzed to obtain the related orientational distribution function $f(\cos\theta)$ and hence, the order parameters $\langle P_L \rangle$, (L = 2, 4).

Experimental technique and data analysis

X-ray diffraction studies were carried out at the Institute of Physical Chemistry, Martin-Luther-University Halle-Wittenberg, Halle (Saale), Germany. For the symmetric bent-core compounds, measurements were performed on oriented samples under the influence of a magnetic field (B ≈ 1 T) using thin capillaries. The alignment was preserved by slow cooling at a rate of 0.1 °C min^{-1} in the presence of the applied magnetic field. For the hockey-stick shaped compounds, surface-aligned samples were obtained by slowly cooling a drop of the liquid crystal placed on a glass plate on a temperature controlled heating stage and the X-ray beam was directed parallel to the glass plate. In both the cases, the resulting patterns were recorded by a 2D area detector (HI-STAR, Siemens AG/Bruker) using Ni-filtered Cu-K_α radiation.

Orientational distribution functions and order parameters

The orientational distribution function $f(\beta)$ of a mesogenic medium describes how the molecular long axes are distributed about the director $\hat{n}$. It

gives the probability of finding a molecule at some prescribed angle β related to $\hat{n}$. The scattered intensity profile $I(\chi)$ (χ presents the azimuthal angle) of the outer diffused equatorial arc of an oriented sample may be analyzed to obtain the related orientational distribution function and order parameter values. According to Leadbetter and Norris [16],

$$I(\chi) = C \int_{\beta=\chi}^{\pi/2} f_d(\beta) \sec^2 \chi \, [\tan^2 \beta - \tan^2 \chi]^{-1/2} \sin \beta \, d\beta \qquad (2.1)$$

where, $f_d(\beta)$ is the distribution function for an orientation β of a local cluster of molecules relative to the director $\hat{n}$ (β = 0). Equation (2.1) can be numerically inverted to give $f_d(\beta)$ which is assumed to be close to the singlet distribution function $f(\beta)$. The orientational order parameters $\langle P_2 \rangle$ and $\langle P_4 \rangle$ are related to the average orientation of the molecular long axes with respect to the director as:

$$\langle P_L \rangle = \frac{\int_0^1 P_L(\cos\beta) f_d(\beta) d(\cos\beta)}{\int_0^1 f_d(\beta) d(\cos\beta)} \qquad (2.2)$$

where, L = 2, 4.

To calculate $f_d(\beta)$ and hence, the order parameter one requires $I(\chi)$ in one quadrant (e.g., from χ = 0 to χ = 90°). In this work the $I(\chi)$ values have been analyzed in multiple quadrants (either two or four depending on shadowing of the pattern due the heating stage) separately and the average values of $I(\chi)$ have been considered to evaluate $f_d(\beta)$ and hence, $\langle P_2 \rangle$ and $\langle P_4 \rangle$ for all the samples. The error in the determination of $\langle P_2 \rangle$ and $\langle P_4 \rangle$ has been estimated to be within ± 0.015.

Apparent molecular length or layer spacing

The apparent molecular length (l) or layer spacing (d) is related to the corresponding Bragg angle (θ_d) through to the formula [17]:

$$2d \sin \theta_d = \lambda \qquad (2.3)$$

where, θ_d is the Bragg angle for the meridional diffraction crescent or spots and λ is the wave length of the X-ray. The first order meridional diffraction peaks were used for calculating the *l* or *d* values as the second order reflections were either very weak or absent.

2.2.4. ^{13}C NMR measurement

NMR measurements were performed on a Bruker Avance III 600 MHz NMR spectrometer (Bruker Biospin) operating at resonance frequency of 600.15 MHz for ^{1}H and 150.93 MHz for ^{13}C resonance at the Centre of Bio-Medical Research, SGPGIMS Campus, Lucknow, Uttar Pradesh. All the experiments were carried out on a 3.2 mm DVT probe under static conditions. Proton decoupled one dimensional carbon spectra were recorded using a single pulse. SPINAL128 scheme was used for realizing the proton decoupling during the acquisition. The carbon and proton $\pi/2$ pulse length were 2 μs and 2.6 μs respectively. Proton decoupled ^{13}C spectra at different temperatures were recorded with 2*k* data points, a spectral width of 301 ppm and a proton decoupling field of 96 kHz. The ^{1}H decoupling field offset was 4 ppm. To avoid radio frequency overheating of the sample, 10 s recycle delay time was used. For ^{13}C experiments in the mesophases, the samples were uniformly aligned by slow cooling from the isotropic to the nematic phase in the presence of a magnetic field. The sample-temperature was regulated with the help of a Bruker temperature controller unit. Measurements were performed during cooling, waiting for at least 20 minutes before the acquisition of each spectrum to ensure temperature stability.

To facilitate the determination of temperature dependence of orientational order parameter ($S = \langle P_2 \rangle$), the 1D ^{13}C NMR spectra were recorded in different mesophases of the investigated compounds. From an analysis of the chemical shifts for a few selected carbon nuclei in the mesogenic molecule the order parameter can be evaluated [21–23] based on the assumption that the molecular order can be described by a single order

parameter. Since the main concern of this work was to investigate the variation in the order parameter across the phase transitions, the C–H order parameters of the aliphatic chains were not studied because their changes were smaller than those of the aromatic core.

2.2.5. Optical birefringence measurement

The nematic liquid crystals usually behave as an optically uniaxial birefringent medium with a uniform orientation of the molecular director and hence, can be characterized by two principal refractive indices viz. the ordinary refractive index (n_o) and the extraordinary refractive index (n_e), perpendicular and parallel to the molecular long axis respectively. The birefringence (Δn) is defined as:

$$\Delta n = n_e - n_o \tag{2.4}$$

In this study, optical birefringence measurements have been accomplished by two different methods. In the first method, the ordinary (n_o) and the extraordinary (n_e) refractive indices were measured by thin prism technique [24, 25] and from the measured n_o, n_e values, the birefringence (Δn) was calculated. In the other method, a high resolution temperature scanning measurement of the optical phase retardation ($\Delta\varphi$) was used to determine the temperature dependence of birefringence of liquid crystalline samples in different mesophases [26–30].

2.2.5.1. Thin prism technique

In this method, the principal refractive indices (n_o, n_e), the average refractive index $n_{av} = \sqrt{\{(2n_o^2+n_e^2)/3\}}$ and the birefringence (Δn) for wave length λ = 632.8 nm (He–Ne laser) were measured within an accuracy of ±0.0006. Hollow prisms with refracting angle less than 2° were constructed using optically flat glass slides. The samples were filled into the prisms in their isotropic state and repeatedly made to pass through few slow heating and cooling cycles between their isotropic and mesogenic states for obtaining

proper alignment with the long axis of liquid crystal molecules parallel to the refracting edges. The prism was placed within a specially constructed brass heater positioned between the pole pieces of an electromagnet with an available magnetic field of about 1T, the temperature of which was controlled by a Eurotherm PID 2404 process controller with an accuracy of ±0.1 °C. The schematic representation of the experimental set-up is shown in figure 2.2. While passing through the aligned liquid crystal medium, the light beam splits into the ordinary and extraordinary components, thereby producing two spots on the screen. The images of the spots were recorded using a digital camera suitably interfaced with a computer. The high-resolution digital images so obtained were further processed to locate the centre of the spots from where the ordinary (n_o) and extraordinary (n_e) refractive indices could be determined. Before introducing the samples, the angle of the prisms were determined by filling them with ultrapure degassed water and measuring the deviations produced in the light beam.

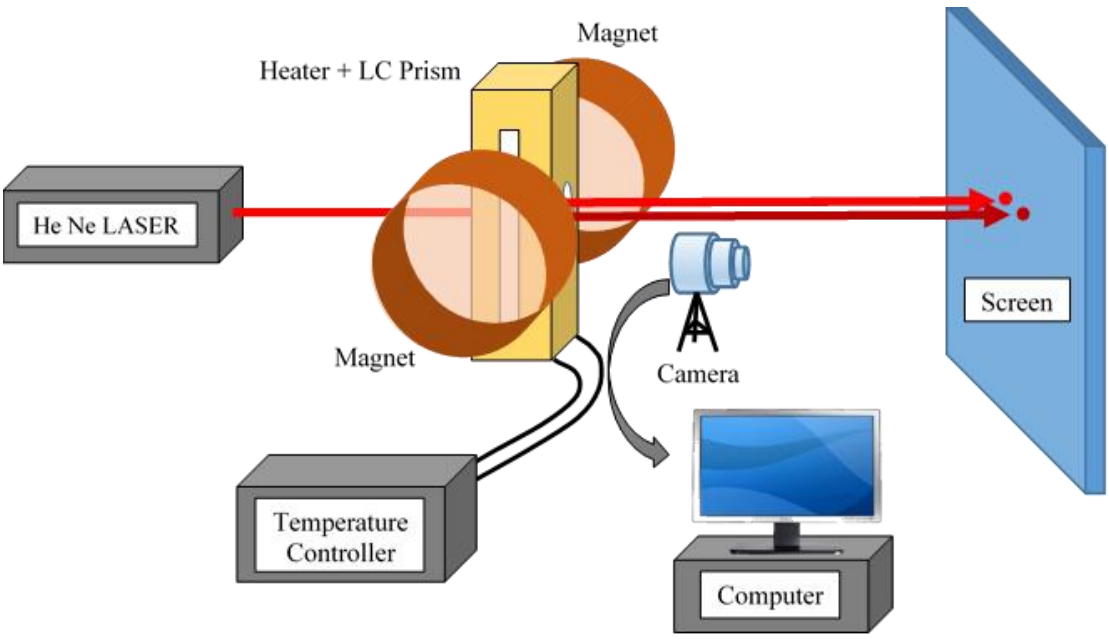

Figure 2.2. Schematic diagram of the experimental set-up for refractive index measurement from thin prism technique.

To construct the hollow prisms, optically flat glass slides were taken and cut to proper dimensions. They were then cleaned with detergent and water and

treated in an acid mixture (conc. H_2SO_4 + conc. HNO_3) at 60 °C for one hour. Next the slides were washed with distilled water and treated with 1 molar solution of KOH at 60 °C for one hour. Then they were rinsed thoroughly with distilled water for several times and left in acetone for few hours to remove any residual impurity. Next one surface of each of the slides was treated with dilute solution of polyvinyl alcohol and after drying rubbed for several times (40–50 times) with filter paper for achieving suitable planar alignment. A thin glass spacer was introduced between the surfaces at one of the vertical edges of the prism so as to attain the desired refracting angle which was kept less than 2°. The glass plates were then sealed using a high temperature adhesive and after curing were baked for several hours in an oven at about 100 °C.

2.2.5.2. Optical transmission method

In optical transmission method, precise measurement of the optical birefringence (Δn) have been accomplished by measuring the intensity of a laser beam transmitted through a planar aligned liquid crystal filled cell of suitable thickness and then measuring the related phase retardation ($\Delta\varphi$). A He–Ne laser (λ = 632.8 nm) beam was employed for this purpose. The cell was placed in a custom built brass heater between two crossed linear polarizers (Glan-Thomson) and its temperature was simultaneously regulated and measured with the aid of a temperature controller (Eurotherm PID 2404) with a resolution of ±0.1 °C [figure 2.3]. To attain a better thermal stability, a two-stage heating arrangement was employed by placing the heater inside another oven. The temperature of the outer oven was controlled by another temperature controller (Eurotherm PID 2404). Typically a temperature difference of about 3–5 K was maintained between the inner and outer ovens. During measurement, the transmitted light intensity was acquired with the aid of a photo diode at an interval of 2 or 3 s while the heater temperature was varied at a rate of 0.5 °C min^{-1}. This translates into a temperature difference of 0.017 °C and 0.025 °C between two successive readings respectively. Furthermore, the

stability of the LASER intensity was monitored by feeding a fraction of the emergent light obtained by a beam splitter to another identical photodiode.

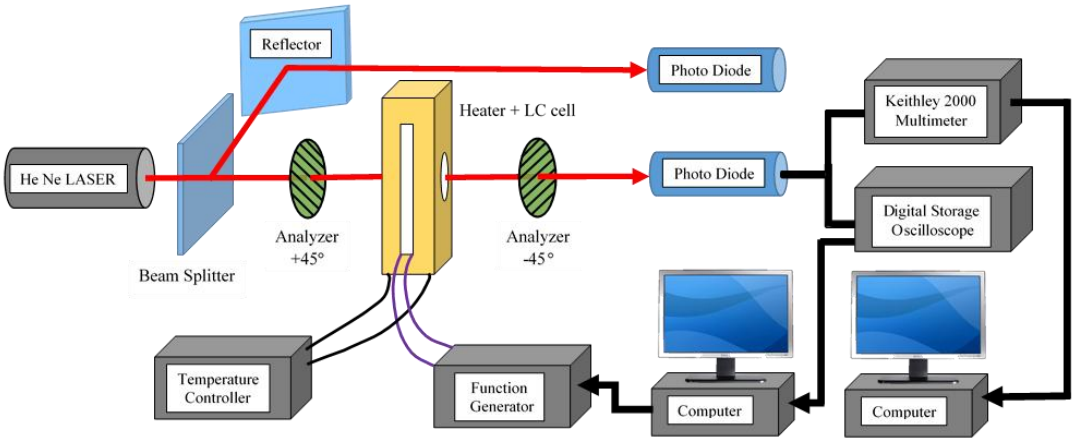

Figure 2.3. Schematic diagram of the experimental set-up for optical transmission measurement.

The normalized light intensity or transmittance when expressed in terms of the phase retardation ($\Delta\varphi$), may be given as [26]

$$I_t = \frac{\sin^2 2\theta}{2}(1 - \cos\Delta\varphi) \tag{2.5}$$

where θ is the angle made by the polarizer with the optic axis and the phase retardation is given by

$$\Delta\varphi = \frac{2\pi}{\lambda}\Delta nd \tag{2.6}$$

where $\Delta n = n_e - n_o$, n_e and n_o being the two principal refractive indices of the liquid crystal medium, λ is the wave length of the light used and d is the sample thickness. For optimizing the measurement, θ was kept at 45°.

The transmitted intensity is an oscillatory function with maxima and minima occurring for $\Delta\varphi = (2m+1)\pi$ and $2m\pi$, where m is an integer. Analyzing the intensity data accordingly, the birefringence values may be evaluated from the resultant phase retardation provided λ and d are known [27–30].

In this work, planar or homogeneously aligned (HG) and homeotropically aligned (HT) standard indium-tin oxide (ITO) coated cells of thicknesses 5 μm and 8.9 μm (procured from AWAT PPW, Warsaw, Poland) were used for the different samples. The empty cells were heated to 5 °C –10 °C above the sample clearing temperature and then the samples were introduced via capillary action. To ensure proper alignment, the sample filled cells were observed under the polarizing optical microscope (Motic BA 300) in all the investigated mesophases. All the measurements were carried out for several cooling and heating cycles and reproducible results were obtained. The sensitivity in Δn values was found to be better than 10^{-5} for the 5- μm-thick sample. This method was also extended to the Sm-*A* and Sm-*C* phases of the liquid crystalline materials.

Determination of orientational order parameter

The orientational order parameter ($S = \langle P_2 \rangle$) of a mesogenic medium can conveniently be determined with the aid of both the principal refractive indices (n_o,n_e) and the birefringence (Δn) values. However, the evaluation of order parameter from the refractive indices data necessitates corresponding density (ρ) values of the material as a function of temperature, wherein an application of the isotropic internal field model by Vuks, Chandrasekhar and Madhusudana (VCM model) [31, 32] or the anisotropic internal field model of Neugebauer, Maier, and Saupe (NMS model) [33–35] leads to the evaluation of the longitudinal (α_l) and transverse (α_t) components of polarizibilities with reference to the long molecular axis. From the measured temperature dependence of the polarizability anisotropy ($\Delta\alpha$) and by applying the well-known Haller's extrapolation [36], the anisotropy in the perfectly ordered state ($\Delta\alpha_0$) and hence, the order parameter (S) of the medium can be determined from the relation $\langle P_2 \rangle = \Delta\alpha/\Delta\alpha_0$. However, in general, the variation of density (ρ) over the nematic range is relatively small [37] and the birefringence (Δn) itself is a quite good description of the orientational ordering of the medium

and can directly be used to determine the order parameter (*S*) [28–30, 38–40]. There are also reports demonstrating consistency between the order parameter (*S*) values extracted from polarizibility and birefringence data [41]. In this study, the assessment of order parameter (*S*) has been accomplished from the analysis of the birefringence data only.

The order parameter is defined as

$$\langle P_2 \rangle = \Delta n / \Delta n_0 \tag{2.7}$$

where Δn_0 is the birefringence in the completely ordered state and was obtained from the temperature dependence of Δn, which can be approximated well for liquid crystals by [36]

$$\Delta n = \Delta n_0 \left(1 - \frac{T}{T^*}\right)^{\beta} \tag{2.8}$$

where Δn_0, T^* and β are adjustable parameters. T^* is about 1–2 K above the clearing temperature. The exponent β depends on the molecular structure and its value is close to 0.2. It may be mentioned that the resolution of the birefringence values obtained from the optical transmission technique is relatively much higher than those determined from thin prism measurements. Hence, the temperature dependence of Δn from the former method can be used for a quite precise estimation of $<P_2>$ values within the mesophases, whereas the limiting behavior of the same can be analyzed for a faithful manifestation of the pretransitional fluctuations and also the nature of different phase transitions in liquid crystals [30, 38–40].

2.2.6. Static dielectric permittivity measurement

The temperature variation of static dielectric permittivities $\varepsilon_{\parallel}$ and $\varepsilon_{\perp}$ along and perpendicular to the molecular long axis respectively, and the dielectric anisotropy $\Delta\varepsilon$ (= $\varepsilon_{\parallel}$-$\varepsilon_{\perp}$) and average dielectric permittivity {ε_{avg} = 1/3($2\varepsilon_{\perp}+\varepsilon_{\parallel}$)} were determined by measuring the capacitance of suitably aligned liquid crystal filled cells at a frequency of 1 kHz, using a precision digital

LCR-bridge (Agilent 4980A) with a relative accuracy of ±0.05% [42]. For this purpose, planar or homogeneously aligned (HG) and homeotropically aligned (HT) standard indium-tin oxide (ITO) coated cells of thicknesses 5 μm and 8.9 μm (procured from AWAT PPW, Warsaw, Poland) were used. The liquid crystalline materials were introduced in the cells in the isotropic phase by capillary action. The cells were placed in a specially constructed electrically powered thermostat-block, the temperature of which was controlled within an accuracy of ±0.1 °C by a process controller (Eurotherm PID 2404). The stray capacitances of the cells were determined by measuring the capacitance of spectroscopic grade pure benzene and *para*-xylene. If C_0 presents the capacitance of the air-filled cell and C_a is that of the empty cell excluding the stray capacitance C_S, then one can write

$$C_0 = C_a + C_s \tag{2.9}$$

For a fluid of dielectric permittivityε, the above equation modifies to

$$C = \varepsilon C_a + C_s \tag{2.10}$$

where C presents the capacitance of the cell filled with the fluid. From equations (2.9) and (2.10) the stray capacitance C_s and hence, the dielectric permittivity can be evaluated following

$$\varepsilon = \frac{C - C_s}{C_0 - C_s} \tag{2.11}$$

The accuracy of the setup had been validated by measuring the dielectric permittivities of the compounds 5CB and 7CB, which were found to be in close agreement with those reported in the literature [43].

2.2.7. Dielectric spectroscopy measurement

To study the frequency dependant dielectric behavior, measurements of the real (ε') and the imaginary (ε'') parts of the complex dielectric permittivity were carried out in the frequency range from 0.1 Hz to 10 MHz with the aid of an impedance analyzer Solartron SI 1260 (Schlumberger) at the Institute of

Chemistry–Physical Chemistry, Martin-Luther-University Halle-Wittenberg, Halle (Saale), Germany. The samples were filled in a gold coated double plate condenser with plate-separation equal to 0.1 mm and oriented in the nematic phase by application of an external magnetic field parallel (p) and perpendicular (s) to the director. However, in the Sm-*C* phases these symbols only point to the starting orientation because the actual orientation of the molecules with respect to the measuring electrical field is not known. The change in capacitance (*C*) and conductance (*G*) of the sample filled condenser can directly be related to the real and imaginary parts of the permittivity of the sample as

$$\varepsilon' = \frac{C - C_s}{C_0 - C_s} \tag{2.12}$$

$$\varepsilon'' = \frac{G}{2\pi f C_0} \tag{2.13}$$

where C_0 presents the capacitance of the air-filled condenser and C_s presents the stray capacitance.

2.2.8. Elastic constant measurement

In a nematic liquid crystal the average alignment of molecules in a region of space can suitably be described by a unit vector $\hat{n}$, called the 'director'. Under the influence of external perturbing fields or even thermal agitations, the relative orientations of the liquid crystal molecules may undergo a change from their equilibrium configuration and the related deformations can conveniently be accounted for by adopting the concept of vector field of the director. The restoring torques, which are developed here are assumed to oppose the curvature of the director field and are termed as the restoring stresses [44]. The free energy of this deformed state is evidently higher from that in the equilibrium state and can be expressed as a quadratic function of the curvature strains with the related elastic moduli appearing as coefficients in it.

Theoretically, the curvature of director (i.e., deformation produced under the influence of external perturbations) can best be described by the continuum theory, the foundation of which was developed by Oseen [45] and Zocher [46]. Later Frank revisited the problem and presented it as a theory of curvature elasticity [44]. Depending on modes of elastic deformations, it can be shown that there exist three independent elastic constants [37, 47–50] for a uniaxial nematic liquid crystal.

According to the continuum theory of liquid crystals [50], the elastic part of free energy density of the deformed state may be expressed as

$$F_{def} = \frac{1}{2}\left[K_{11}\left(\vec{\nabla}.\hat{n}\right)^2 + K_{22}\left(\hat{n}.\vec{\nabla}\times\hat{n}\right)^2 + K_{33}\left(\hat{n}\times\vec{\nabla}\times\hat{n}\right)^2\right] \quad (2.14)$$

where the constants K_{11}, K_{22}, and K_{33} are termed as the splay, twist and bend elastic constants respectively and collectively termed as the Frank elastic moduli. The elastic moduli possess the dimension energy length^{-1}. Each term in the right hand side of the equation (2.14) represents the contributions from the related mode of deformation [figure 2.4] and therefore possesses non-vanishing magnitude when the corresponding distortion is present. Furthermore, as each of these deformations can be induced separately, i.e., pure splay, pure twist or pure bend deformation; hence, each of K_{11}, K_{22}, and K_{33} must be positive [48].

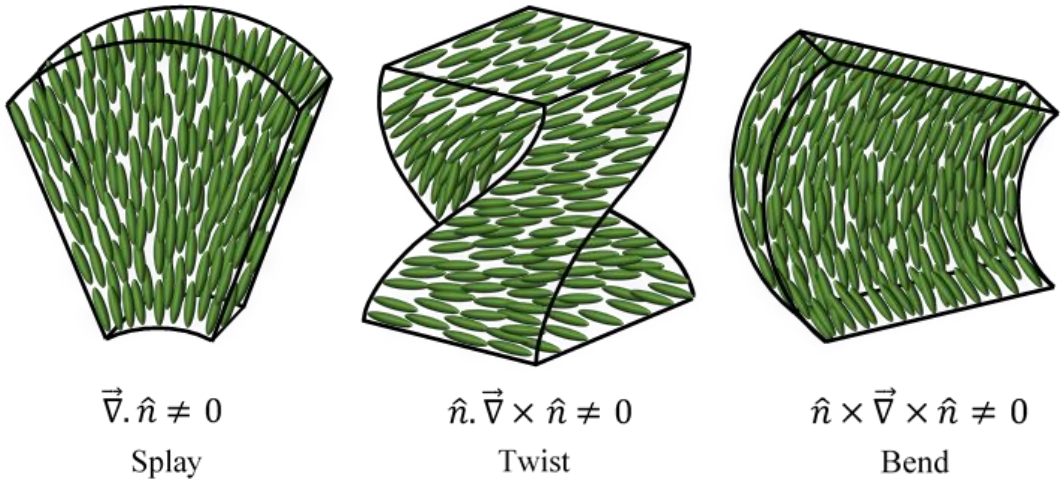

Figure 2.4. The three different types of director deformation in a nematic liquid crystal.

The elastic moduli of the liquid crystalline materials can be determined with the aid of several techniques. One of the most simple and convenient one is the observation of critical electric or magnetic fields required for different types of Freedericksz transition [51]. The term Freedericksz transition refers to the deformation of a uniformly aligned thin layer of nematic liquid crystal in an external electric [52–54] or magnetic field [55–59]. If a planar surface aligned nematic liquid crystal with positive diamagnetic or dielectric anisotropy is subjected to an external electric or magnetic field in a direction normal to the director and having magnitude greater than the threshold or critical value, the director of the sample starts to orient along the applied field direction. Depending on the geometry of the arrangement, one can be able to determine the splay, twist or bend elastic constants from Freedericksz transition under the influence of an external field.

In this work, the splay elastic constant (K_{11}) measurements have been performed by studying the electric field induced Freedericksz transition, i.e., from an inspection of the capacitance-voltage characteristics of the sample in the nematic phase [figure 2.5], the initial planar alignment being distorted by an electric field parallel to the substrate normal. A thin layer of the nematic sample contained in a planar aligned (HG) standard indium-tin oxide (ITO) coated cells of thicknesses 5 μm or 8.9 μm was subjected to an external sinusoidal voltage of frequency 1 kHz. The magnitude of the applied voltage was gradually increased at intervals of 20 $mV_{r.m.s.}$ from a value lower than Freedericksz threshold (V_{th}) voltage to a maximum of 20 $V_{r.m.s}$. [limiting field offered by the function generator (Picotest G5100A) used]. The variation of capacitance of the sample-filled cell was studied with the help of the precession LCR meter Agilent 4980A, from which the Freedericksz threshold voltage could be determined (within an accuracy of ±5%) provided V_{th} is much smaller than the maximum applied voltage. From the knowledge of the dielectric anisotropy $\Delta\varepsilon$, splay elastic constant K_{11} could be ascertained using the following relation:

$$K_{11} = \frac{\varepsilon_0 \Delta\varepsilon V_{th}^2}{\pi^2} \qquad (2.15)$$

where ε_0 is the permittivity of free space and V_{th} is the critical field in r.m.s.

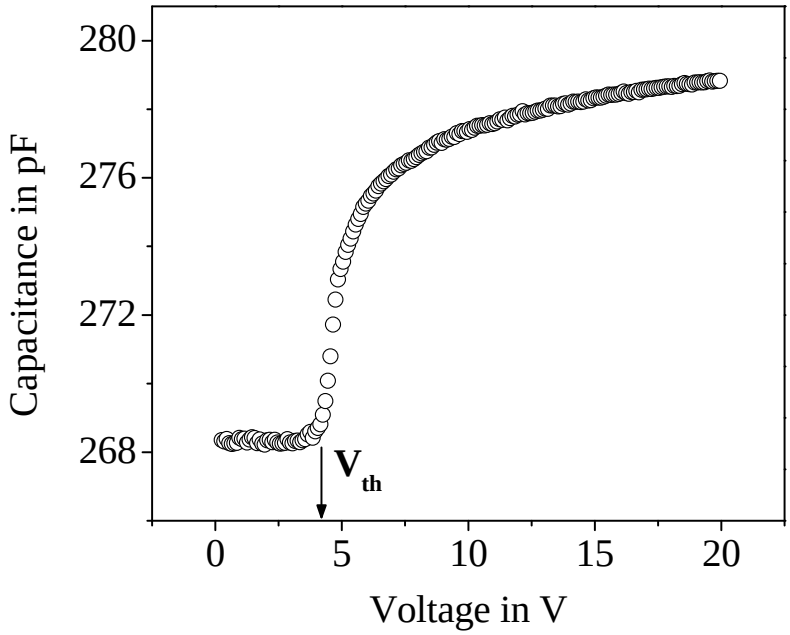

Figure 2.5. Voltage dependent variation of sample filled cell-capacitance due to electrically driven Freedericksz transition in bent-core compound **1**/**7** (described in chapter 3) at 103 °C.

The bend elastic constant K_{33} was determined from an analysis of the dependence of the cell capacitance on the voltage sufficiently above the threshold value [60]. The equation describing the voltage (V) dependent capacitance $C(V)$, was first introduced by Gruler, Scheffer and Meier [52] and was subsequently modified by Uchida and Takahashi [61]. The final expression describing the $C(V)$ dependence may be given as [62, 63]:

$$\frac{C(V)-C_\perp}{C_\perp} = \gamma - \frac{2\gamma}{\pi}\frac{V_{th}}{V}\sqrt{1+\gamma\, sin^2\,\varphi_m}$$

$$\times \int_0^{\varphi_m} \left\{\frac{(1+\kappa\, sin^2\,\varphi)(1-sin^2\,\varphi)}{(1+\gamma\, sin^2\,\varphi)(sin^2\,\varphi_m - sin^2\,\varphi)}\right\}^{\frac{1}{2}} cos\,\varphi d\varphi \qquad (2.16)$$

where, $\kappa = K_{33}/K_{11}$-1, $\gamma = \varepsilon_{\parallel}/\varepsilon_{\perp}$-1, φ is the tilt angle between the director $\hat{n}$ and the cell wall, φ_m is the tilt angle at the centre of the cell and $C_{\perp}$ is the capacitance of the cell when the liquid crystal molecules are homogeneously aligned.

For a field much higher than the threshold value (V_{th}), $\varphi_m = \pi/2$ and hence, equation (2.16) assumes the form

$$\frac{C(V)-C_{\perp}}{C_{\perp}} = \gamma - \frac{2\gamma}{\pi}\frac{V_{th}}{V}\sqrt{1+\gamma} \times \int_0^{\pi/2} \left\{\frac{(1+\kappa \sin^2\varphi)}{(1+\gamma \sin^2\varphi)}\right\}^{\frac{1}{2}} \cos\varphi d\varphi \quad (2.17)$$

From equation (2.17) it is evident that for $V >> V_{th}$, a $(C\text{-}C_{\perp})/C_{\perp}$ *vs* $1/V$ plot should be linear with a slope

$$\alpha = \frac{2\gamma}{\pi}\sqrt{1+\gamma}V_{th} \times \int_0^{\pi/2} \left\{\frac{(1+\kappa \sin^2\varphi)}{(1+\gamma \sin^2\varphi)}\right\}^{\frac{1}{2}} \cos\varphi d\varphi \quad (2.18)$$

The extrapolation of the curve to $1/V = 0$ yields directly the value of $\gamma = \Delta\varepsilon/\varepsilon_{\perp}$. Therefore, by measuring α and γ, the parameter κ and hence, the elastic constant K_{33} can easily be evaluated when the values of K_{11} are available. These procedures enable to determine the K_{11} and K_{33} values with an accuracy of around ±3% and ±8% respectively.

2.2.9. Rotational viscosity measurement

The rotational viscosity (γ_1) of liquid crystalline compounds is an important parameter in relation to the dynamics of LC molecules and is related to the torque associated with rotation of liquid crystal molecules in an external perturbing field. It describes the force of internal friction among directors during such rotational motion and has been found to depend on the structural form and constitution of the liquid crystal molecules, their intermolecular interactions and sample temperature.

For the determination of rotational viscosity, the splay elastic constant (or bend elastic constant for compounds with negative dielectric anisotropy) as well as the relaxation time of the sample is required. In this study,

measurements of relaxation time have been conducted by two different probing methods *viz.* capacitive decay and optical phase-decay-time measurement methods which also permits a precise comparison between the two sets of values.

2.2.9.1. Optical method

A relaxation method involving the time decay of optical phase retardation was undertaken to determine the rotational viscosity coefficient (γ_1) [64–69]. A small voltage was applied to a planar aligned liquid crystal filled cell to deform the nematic directors by a small angle. On the removal of the field at time t = 0, the director reorients due to the relaxation of elastic distortions with a characteristic relaxation time τ_0. For a liquid crystal filled homogeneously aligned cell of thickness d, γ_1 may be expressed as

$$\gamma_1 = \frac{\tau_0 K_{11} \pi^2}{d^2} \tag{2.19}$$

where K_{11} presents the splay elastic constant of the liquid crystal.

From a measurement of the transmitted light intensity through a homogeneously aligned LC cell, the optical phase retardation may be obtained as a function of time. Assuming that the LC directors are deformed on the application of voltage by a small angle, the decay time is approximated by the following equation [64]

$$\delta(t) \cong \delta_0 \exp(-2t/\tau_0) \tag{2.20}$$

where δ_0 is the total phase change of the LC cell under a bias voltage V_B. When δ_0 is close to an integral value of π, then the expression for $\delta(t)$ becomes [65]

$$\delta(t) \cong \delta_0 \exp(-4t/\tau_0) \tag{2.21}$$

A plot of $\ln[\delta_o/\delta(t)]$ is linear in time, with a slope equal to either $2/\tau_0$ or $4/\tau_0$, from which the relaxation time could be evaluated. The accuracy of the relaxation time measurement was found to be within ±5ms.

A He-Ne laser (λ = 632.8 nm) was passed through a homogeneously aligned ITO coated LC cell (AWAT PPW, Poland) placed between two crossed polarizers oriented at 45° to the director [figure 2.6]. The cell was placed in a specially constructed brass heater, the temperature of which was regulated and measured with an accuracy of ± 0.1 °C by a process controller (Eurotherm PID 2404). The transmitted light intensity was measured as a function of applied voltage using a photodiode which exhibited maxima and minima [figure 2.7(a)]. A voltage corresponding to the first maximum or minimum in the transmitted intensity was then applied to the LC cell to distort the director. On the removal of this voltage V_B, the director relaxes back and the transmitted light intensity change ($I(t)$) during this process was recorded by a photo diode connected to a digital storage oscilloscope (DSO) [figure 2.7(b)].

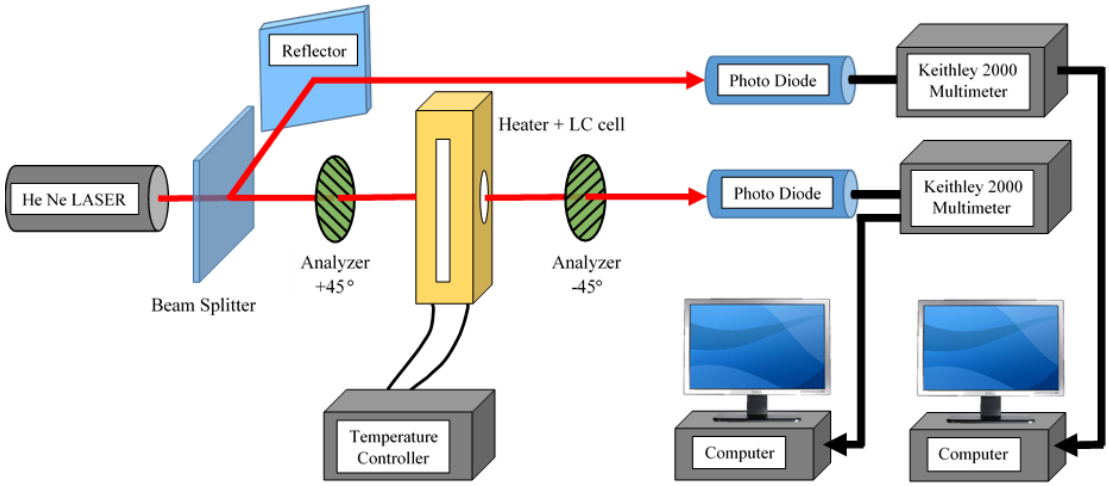

Figure 2.6. Schematic diagram of the experimental set-up for rotational viscosity measurement.

The accompanying phase retardation $\delta(t)$ could be calculated from the time-dependent intensity ($I(t)$) using the following equation:

$$I(t) = I_0 \sin^2\{(\Delta_{tot} - \delta(t))/2\} \qquad (2.22)$$

where I_0 is the maximum intensity change and $\Delta_{tot} = (2\pi/\lambda)\,\Delta n.d$ is the total optical phase retardation which was calculated from the birefringence measurement. By knowing $\delta(t)$ the relaxation time was calculated from the

slope of the ln[$\delta_0/\delta(t)$] *vs* time plot. Hence, by measuring the relaxation time τ_0 and the splay elastic constant K_{11} and knowing the cell gap d, the rotational viscosity γ_1 could be ascertained.

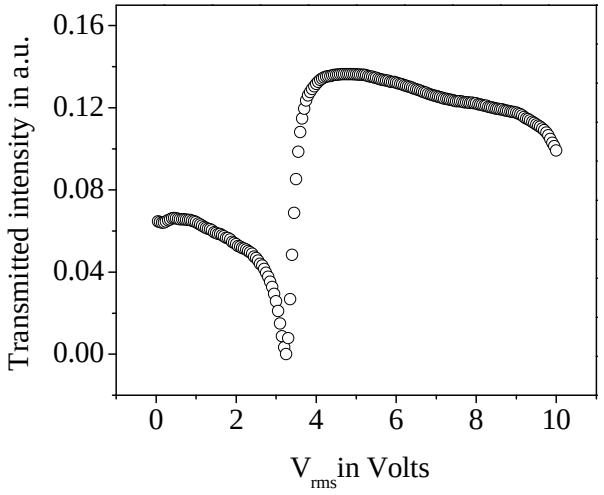

(a)

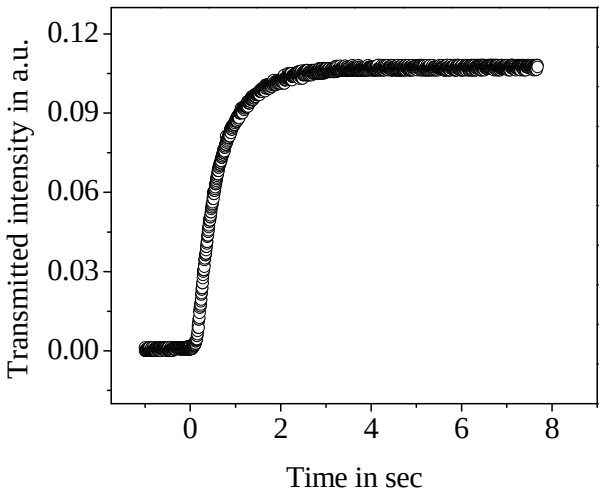

(b)

Figure 2.7. (a) Voltage dependent transmittance for the bent-core compound **1/7** (described in chapter 3) placed inside an 8.9 μm thick homogeneously aligned liquid crystal cell at 109 °C; (b) Time dependent variation of intensity for compound **1/7** at 109 °C, when bias voltage is removed instantaneously.

2.2.9.2. Capacitance method

In capacitance method, the LC director reorientation time (τ_0) and hence, the rotational viscosity coefficient (γ_1) was measured using a digital impedance analyzer (Agilent 4980A) in programmable mode and with suitable computer interfacing which provides a capacitive decay of the sample against time. The sample was filled in a homogeneously aligned LC cell consisting of two indium-tin oxide (ITO) coated glass plates with spacing of 5 μm or 8.9 μm. The operating frequency was kept fixed at 10 KHz. As the decay processes in bent-core or hockey stick-shaped compounds are comparatively slow, a delay time of 30 ms – 100 ms was introduced between successive readings. Now, an ac voltage (V) greater than the corresponding Freedericksz threshold voltage (V_{th}) was applied ($V/V_{th} \approx 2.5$) across the cell for a time of about 1 minute. On sudden lowering of the field to a value about 200 $mV_{r.m.s.}$ ($<V_{th}$), the LC directors relax back to their initial configuration and accordingly the effective cell-capacitance changes. For such a change it has been found that in small signal regime the difference between the instantaneous capacitance (C_t) at a particular time t and the equilibrium state capacitance ($C_\perp$) (for homogeneous alignment) follows [70] the following simple exponential decay form

$$\Delta C_t = C_t - C_\perp = \Delta C_0(exp(-2t/\tau_0)) \qquad (2.23)$$

where $\Delta C_0 \approx C_\perp(\Delta\varepsilon/2\varepsilon_\perp)\varphi_m$ for planar alignment of the LC molecules, $\varepsilon_\perp$ is the static dielectric permittivity perpendicular to the molecular long axis, $\Delta\varepsilon$ is the dielectric anisotropy, $C_\perp$ is the capacitance of the cell when the liquid crystal molecules are homogeneously aligned and φ_m is the director tilt angle at the middle of the layer at time t = 0, i.e., when the relaxation initiates. The experimental results of Schad [70] show that equation (2.23) is a good approximation for $\varphi_m < 1$.

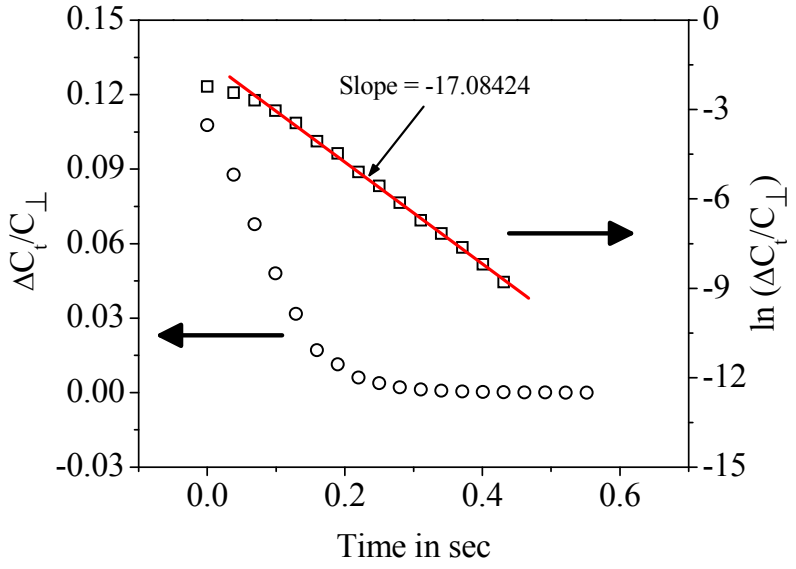

Figure 2.8. Transient capacitance response of hockey stick-shaped compound **2** (described in chapter 5) placed inside a homogeneously aligned LC cell at 103.5 °C. $\Delta C_t/C_\perp$ and ln ($\Delta C_t/C_\perp$) are plotted against time.

Figure 2.8 represents an example of the transient capacitance response for reorientation of LC directors after removal of the applied electric field. To study the switching behavior, the variation of transient capacitance was recorded against time at different temperatures. From the slope of the logarithmic plot of $(C_t - C_\perp)/C_\perp$ against time, relaxation time (τ_0) could be yielded which lead to the determination of rotational viscosity coefficient (γ_1) following equation (2.19). The same procedure was utilized for negative dielectric anisotropic sample, using homeotropic alignment and by replacing $C_\perp$ by $C_\parallel$ and $\varepsilon_\perp$ by $\varepsilon_\parallel$.

2.2.10. Electro-optical measurement

The electro-optical measurements have been carried out using commercially available polyimide coated ITO test cells (AWAT Co PPW, Poland) having thickness of 5 μm and an active area of 0.25 cm^2. Such a cell-thickness is sufficient to suppress the helical superstructure appearing in the Sm-C* and Sm-C_A* phases to ensure book-shelf geometry. For obtaining good

planar alignment, the sample-filled cells were slowly cooled from the isotropic state and on entering the Sm-*A* phase, were subjected to a sufficiently high square wave field of ~ 8 V μm^{-1} at a frequency of 20 Hz. In this work, measurements of spontaneous polarization were carried out from the polarization reversal technique [71–74].

The liquid crystal cell may be regarded as a combination of a resistance (*R*) and a capacitor (*C*) connected in parallel. When a voltage *V* is applied to such a cell containing the chiral LC sample, the spontaneous polarization $\overrightarrow{P_S}$ of the medium tends to align itself along the direction of the applied field. When the field reverses, during reorientation of $\overrightarrow{P_S}$, there develops a repolarization current I_P due to the variation in the surface charge on the cell-electrodes. In addition, there exist also two more components of current, I_I and I_C, due to the ionic conduction of the liquid crystal and recharging of cell-capacity respectively. Hence, the net current though the cell may be represented as the sum of these three contributions [72] as

$$I = I_P + I_I + I_C = \frac{dP}{dt} + \frac{V}{R} + C\frac{dV}{dt} \tag{2.24}$$

where, *P* presents the amount of charge induced due to polarization realignment, i.e., the amount of charge induced when the spontaneous polarization (P_s) changes sign after reversal of the electric field. The contributions from I_C and I_I were isolated by proper choice of baseline in the output current response curve using mathematical softwares. The spontaneous polarization (P_s) was obtained by integrating the area (*A*) under the current reversal peak in the following way [74]

$$P_s = \frac{1}{2A}\int Idt \tag{2.25}$$

The measurement of the free relaxation or response time (τ) requires to determine the time ($t_{10\text{-}90}$) taken to change the current from 10% to 90% of the peak value of the hump of the repolarization current response upon switching and is expressed as [74, 75]

$$\tau = \frac{t_{10-90}}{1.8} \tag{2.26}$$

The effective torsional bulk viscosity (η) was obtained using the following relation

$$\eta = P_s E \tau \tag{2.27}$$

where E is the applied electric field. In this study, the free relaxation time and the effective torsional bulk viscosity were determined within an accuracy of ±1 μs and ± 0.9 Pa s respectively.

Furthermore, for ferroelectric liquid crystals, the anchoring energy (F) may be expressed as combination of terms related to the dispersion and polarization contributions. It may be shown that [75–77]

$$F = \int_S \left(\widetilde{W}_D + \widetilde{W}_P\right) d\sigma \tag{2.28}$$

where $\widetilde{W}_D = W_D(P_s n)^2$ and $\widetilde{W}_P = W_P(P_s n)$, W_D and W_P being the dispersion and polarization components of the anchoring strength coefficient respectively and $\vec{n}$ presents the layer normal. Again, the dispersion anchoring strength coefficient is related to the spontaneous polarization (P_s) and the response time (τ) through the following relation [75–79]

$$W_D = \frac{\eta d}{4\tau} \tag{2.29}$$

Thus, measuring the P_s and τ values and knowing the cell thickness d, one can determine the dispersion anchoring strength coefficient (W_D). Moreover, for a sufficiently large cell thickness d, the influence of surface anchoring becomes negligibly small. Under this condition, the threshold field (E_{th}) above which the bi-stable state appears, may be given as [75, 77]

$$E_{th} = \sqrt{W_D}/K \tag{2.30}$$

where K presents the average elastic constant and the contribution from the polarizing part of anchoring energy is assumed to be zero. With increasing anchoring, the threshold value of the field consequently enhances. Now, for a

vanishing contribution from the dispersion part of anchoring energy (i.e., W_D = 0), the expression for bi-stability threshold (E_{th}) assumes the following form [75, 77]

$$E_{th} = \frac{W_P^2}{KP_s} \tag{2.31}$$

Combining equations (2.30) and (2.31), the polarizing anchoring strength coefficient (W_P) may be expressed as [75–79]

$$W_P = \sqrt{P_s \sqrt{W_D}} \tag{2.32}$$

For the determination of the different parameters (i.e., P_s, τ, η, W_D and W_P) from the relaxation voltage curves corresponding to the repolarization current, a square wave field (V_{pp} = 38V, f = 20Hz) was applied across a thin layer of sample, contained in a LC cell [figure 2.9]. The voltage output was taken from a combination of an arbitrary waveform generator (Picotest G5100A) and a voltage amplifier (FLC F20A). The polarization current response thus obtained by reversing the applied field, was fed to an Agilent Digital Storage Oscilloscope (model: 1052B) through a resistance of 1 kΩ, connected in series with the LC cell. Corresponding relaxation data was directly obtained on a computer suitably interfaced to the oscilloscope.

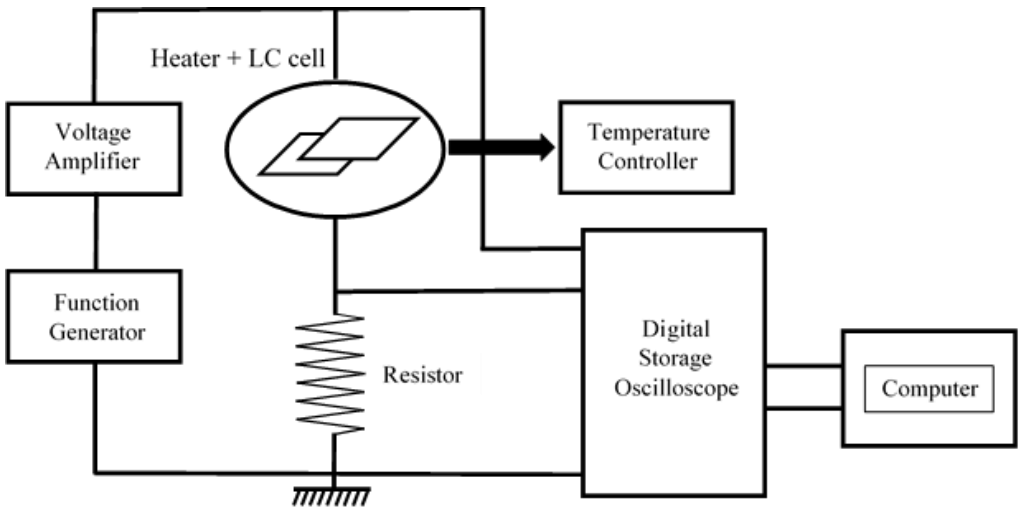

Figure 2.9. Schematic diagram of the experimental set-up for electro-optical study using polarization reversal technique.

2.3. Theoretical background

2.3.1. Maier-Saupe theory

A number of theories have been developed in an attempt to describe the thermodynamic properties of the nematic phase. Among them the most successful and popular are those based on the molecular mean field approximation, being capable of providing qualitative description of many different collective phenomena. However, they face the shortcomings of ignoring intermolecular short-range correlations and fluctuation effects. Maier and Saupe [80–82] proposed a statistical molecular theory of the nematic phase (*N*) and nematic to isotropic (*N–I*) phase transition on the basis of molecular mean field approximation. In this formalism, the molecules are assumed to be under the influence of same average field due to all other molecules in the medium, but otherwise they are uncorrelated with one another. Maier and Saupe also considered that it is the anisotropic part of the dispersion interaction energy between the molecules, originating from the intermolecular dipole–dipole interactions, is responsible for the nematic molecular ordering. However, the contribution from the shape anisotropy of the molecules was totally ignored by them. Maier and Saupe approximated the electrostatic interaction by the first term of its multipole expansion and made the following assumptions

i) The effect of the permanent dipoles can be ignored as far as long range nematic order is concerned.

ii) The effect of the induced dipole-dipole interaction is only needed to be taken under consideration.

iii) The molecules are cylindrically symmetric with respect to their long molecular axis.

iv) Relative to a given molecule, the distribution of the centre of mass of the remaining molecules may be taken as spherically symmetric.

In a liquid crystalline medium, the distribution of the molecular long axis about the director may be specified by an orientational distribution function $f(\cos\theta)$, where θ presents the angle between the director and the molecular long axis. Furthermore, the fact that the rod-like molecules possess head to tail symmetry, makes $f(\cos\theta)$ an even function of $\cos\theta$. Hence, the orientational distribution function $f(\cos\theta)$ may be written as,

$$f(\cos\theta) = \sum_{L-even} \frac{(2L+1)}{2} \langle P_L(\cos\theta)\rangle \, P_L(\cos\theta) \qquad (2.33)$$

where, $P_L(\cos\theta)$ are the L^{th} even order Legendre polynomials, and $< P_L(\cos\theta)>$ are the statistical average given by

$$\langle P_L(\cos\theta)\rangle = \int_0^1 P_L(\cos\theta) f(\cos\theta) d(\cos\theta) \qquad (2.34)$$

$<P_L>$ are termed as the orientational order parameters. Humphries *et al.* [83] introduced a more comprehensive concept by including higher order terms in the mean field potential. Then the single molecule potential function $V(\cos\theta)$ for cylindrically symmetric molecules takes the form,

$$V(\cos\theta) = \sum_{L-even} U_L \langle P_L\rangle \, P_L(\cos\theta) \qquad (L\neq 0) \qquad (2.35)$$

where, U_L are functions of distance between the central molecule and its neighbors only. Inserting, $L = 2$ in equation (2.34) one obtains,

$$\langle P_2(\cos\theta)\rangle = \int_0^1 P_2(\cos\theta) f(\cos\theta) d(\cos\theta) \qquad (2.36)$$

$<P_2>$ in general is termed as the order parameter. For an isotropic liquid $<P_2> = 0$ while for perfectly ordered state (e.g., crystals) $<P_2> = 1$.

Retaining only the first term (i.e., $L = 2$) in the right hand side of equation (2.35), the expression for the a single molecule potential energy assumes the form

$$V(\cos\theta) = -\nu P_2(\cos\theta)\langle P_2\rangle \qquad (2.37)$$

where, $\nu = -U_2$. Hence, the orientational distribution function for a single molecule takes the form

$$f(\cos\theta) = Z^{-1}\exp[-V(\cos\theta)/kT] \tag{2.38}$$

where, k is the Boltzmann's constant and Z presents the single-molecule partition function given as

$$Z = \int_0^1 \exp[-V(\cos\theta)/kT]\, d(\cos\theta) \tag{2.39}$$

Substituting the value of $f(\cos\theta)$ and Z from equations (2.38) and (2.39) respectively into equation (2.36) one can write

$$\langle P_2(\cos\theta)\rangle = \frac{\int_0^1 P_2(\cos\theta)\exp[P_2(\cos\theta)\langle P_2\rangle/T^*]d(\cos\theta)}{\int_0^1 \exp[P_2(\cos\theta)\langle P_2\rangle/T^*]d(\cos\theta)} \tag{2.40}$$

where, $T^* = kT/\nu$.

Equation (2.40) is a self-consistent equation and can be solved to obtain the temperature dependence of $\langle P_2\rangle$. Corresponding to every temperature T^*, there exists one or more values of $\langle P_2\rangle$ that satisfies the self-consistence equation. For a normal isotropic liquid, the value of $\langle P_2\rangle = 0$ and is a solution at all temperatures. In addition, for temperatures $T^* < 0.22284$, two more solutions to equation (2.40) appear. It has been found that the nematic phase with $\langle P_2\rangle > 0$ is the stable one when T^* satisfies the condition $0 \leq T^* \leq 0.22019$. For $T^* > 0.22019$, one obtains a stable isotropic phase with $\langle P_2\rangle = 0$.

With the increase in temperature, the order parameter $\langle P_2\rangle$ exhibits a decreasing trend from unity to a minimum value of 0.4289 at $T^* = 0.22019$. At $T^* = 0.22019$, the *N–I* phase transition takes place and $\langle P_2\rangle$ suffers a discontinuous change from 0.4289 to 0 indicating a first order nature of that transition. However, the entropy change associated with the *N–I* phase transition is only about 0.83 cal K^{-1} $mole^{-1}$, which is much smaller than that of usual solid-liquid transition, which is around 25 cal K^{-1} $mole^{-1}$. Therefore, this transition is often termed as a weakly first order transition. Temperature dependence of $\langle P_2\rangle$ can be obtained by solving equation (2.40) iteratively. Even though a number of approximations and simplifications are adopted in

formulating the Maier-Saupe mean field theory, for a number of nematic liquid crystals, the experimental values of $\langle P_2 \rangle$ have been found to be in good agreement with those predicted by this theory.

2.3.2. McMillan's theory for smectic *A* phase

In addition to the orientational ordering of the molecules, the smectic *A* phase also exhibits a one-dimensional translational ordering of the same. The smectic layers are characterized by a periodic mass-density wave in a direction parallel to the layer-normal **(**say, **z**-direction) and a director (local orientational axis) which is parallel to the **z**-axis. McMillan suggested a simple and elegant description of smectic *A* liquid crystal by extending the Maier-Saupe theory to include an additional order parameter term in the mean field potential energy expression for characterizing the one-dimensional translational periodicity of layered structure [84, 85]. The normalized distribution function can be written as

$$f(\cos\theta) = \sum_{L-even} \sum_n A_{L,n} P_L(\cos\theta) \cos(2\pi n z/d) \qquad (2.41)$$

with the following normalizing condition

$$\int_{-1}^{1} \int_{0}^{d} f(\cos\theta, z)\, dz\, d(\cos\theta) = 1 \qquad (2.42)$$

where, *d* presents the layer thickness.

Following Kobayashi [86–88], McMillan [84, 85] introduced a simple form of the pair interaction potential as

$$V_M(\cos\theta, z) = -v[\delta\alpha\tau \cos(2\pi z/d) + \{\eta + \alpha\sigma \cos(2\pi z/d)\} P_2(\cos\theta)] \qquad (2.43)$$

where, α and δ are the two parameters of the potential. Here, $\eta = \langle P_2(\cos\theta) \rangle$, $\tau = \langle \cos(2\pi z/d) \rangle$, and $\sigma = \langle P_2(\cos\theta) \cos(2\pi z/d) \rangle$ present the orientational, translational and mixed order parameters respectively and <….> denotes the statistical average of the quantities inside.

Hence, the distribution function can be expressed as

$$f_M(\cos\theta, z) = Z^{-1} \exp[-V_M(\cos\theta, z)/kT] \quad (2.44)$$

where, Z is the single molecule partition function and given as

$$Z = \int_0^1 \int_0^{\mathrm{d}} \exp[-V_M(\cos\theta, z)/kT]\, d(\cos\theta) dz \quad (2.45)$$

with k representing the Boltzmann's constant.

Here, three self-consistent equations, containing η, τ and σ are

$$\eta = \int_0^1 \int_0^d P_2(\cos\theta) f_M(\cos\theta, z)\, d(\cos\theta) dz \quad (2.46)$$

$$\tau = \int_0^1 \int_0^d \cos(2\pi z/d)\, f_M(\cos\theta, z)\, d(\cos\theta) dz \quad (2.47)$$

$$\sigma = \int_0^1 \int_0^d P_2(\cos\theta) \cos(2\pi z/d)\, f_M(\cos\theta, z)\, d(\cos\theta) dz \quad (2.48)$$

These equations can be solved iteratively to extract the η, τ and σ values for the different values of the parameters α and δ. Depending on the values of the different parameters, one can obtain the following three possible solutions:

i) $\eta = \tau = \sigma = 0$, corresponds to the disordered phase, i.e., isotropic liquid;

ii) $\eta \neq 0$, $\tau = \sigma = 0$, only orientational order appears, as in nematic phase and in accordance with the Maier Saupe theory;

iii) $\eta \neq 0$, $\tau \neq 0$, $\sigma \neq 0$, orientational and translational order both occurs, as in smectic *A* phase.

For $\alpha > 0.98$, the smectic *A* phase transforms directly into the isotropic phase, while for $\alpha < 0.98$ there exists a nematic–isotropic (*N–I*) transition above the smectic *A*–nematic (Sm-*A*–*N*) transition. According to McMillan theory, the *N–I* transition is always first order. However, the Sm-*A*–*N* transition can be either first order or second order. A (T_{AN} / T_{NI}) value less than 0.87 indicates a second order appearance of the Sm-*A*–*N* transition while for (T_{AN} / T_{NI}) greater than 0.87, the Sm-*A*–*N* transition is of first order. Here, T_{AN} and T_{NI} are the Sm-*A*–*N* and *N–I* transition temperatures respectively.

References:

[1] D. Demus and L. Richter, *Textures of Liquid Crystals*, Verlag Chemie, New York (1978).

[2] I. Dierking, *Textures of Liquid Crystals*, Wiley-VCH Verlag GmbH & Co., Weinheim (2003).

[3] P. Navard and J. M. Haudin, *J. Therm. Anal.*, **30**, 61 (1985).

[4] C. W. Garland, *Liquid Crystals: Experimental Study of Physical Properties and Phase Transitions*, S. Kumar (Ed.), Cambridge University Press, Cambridge (2001).

[5] J. Thoen, *Heat Capacities Liquids, Solutions and Vapours*, E. Wilhelm and T. M. Letcher (Eds.), RSC Publishing, Cambridge (2010).

[6] R. Dabrowski and K. C. Zuprynski, *Advances in Liquid Crystal Research and Applications*, Pergamon Press, Oxford (1980).

[7] H. Stub and W. Perron, *Anal. Chem.*, **46**, 128 (1974).

[8] I. G. Chistyakov, *Sov. Phys. Vsp.*, **9**, 551 (1967).

[9] H. Kelker and R. Hatz, *Handbook of Liquid Crystals*, Verlag Chemie, Weinheim (1980).

[10] L. A. Azaroff, *Mol. Cryst. Liq. Cryst.*, **60**, 73 (1980).

[11] R. H. Templer, *Handbook of liquid crystals*, D. Demus, J. Goodby, G. W. Gray, H.-W. Spiess, V. Vill (Eds.), **Vol. 1**, Wiley-VCH; Weinheim, New York, Chichester, Brisbane, Singapore, Toronto; (1998).

[12] P. Davidson, *Liquid Crystals II* (*Structure and Bonding*), D. M. P. Mingos (Ed.), **Vol. 95**, Springer Verlag, Berlin (1999).

[13] L. M. Blinov, *Structure and Properties of Liquid Crystals*, Springer; Dordrecht, Heidelberg, London, New York; (2011).

[14] B. K. Vainshtein and I. G. Chistyakov, *Problem of Modern Crystallography*, Nauka, Moscow (1975).

[15] A. J. Leadbetter, *The Molecular Physics of Liquid Crystals*, G. R. Luckhurst and G. W. Gray (Eds.), Academic Press, London (1979).

[16] A. J. Leadbetter and E. K. Norris, *Mol. Phys.*, **38**, 669 (1979).

[17] A. de Vries, *Mol. Cryst. Liq. Cryst.*, **10**, 219 (1970).

[18] A. de Vries, *Pramana*, **1**, 93 (1975).

[19] G. Vertogen and W. H. de Jue, *Thermotropic Liquid Crystals: Fundamentals*, Springer-Verlag, Berlin (1988).

[20] H. Kohli *et al., Z. Physik*, **B24**, 147 (1976).

[21] B. Das, S. Grande, W. Weissflog, A. Eremin, M. W. Schröder, G. Pelzl, S. Diele, and H. Kresse, *Liq. Cryst*., **30**, 529 (2003).

[22] H. Sun, M. D. Roth, and B. M. Fung, *Liq. Cryst*., **28**, 1469 (2001).

[23] D. Catalano, L. Chiezzi, V. Domenici, M. Geppi, C. A. Veracini, R. Y. Dong, and K. F. Csorba, *Macromol. Chem. Phys*, **203**, 1594 (2002).

[24] A. K. Zeminder, S. Paul, and R. Paul, *Mol. Cryst. Liq. Cryst.*, **61**, 4191 (1980).

[25] A. Prasad and M. K. Das, *Phase Transitions*, **83**, 1072 (2010).

[26] A. Saipa and F. Giesselmann, *Liq. Cryst.*, **29**, 347 (2002).

[27] T. Scharf, *Polarized Light in Liquid Crystals and Polymers*, John Wiley and Sons, Hoboken (2007).

[28] G. Sarkar, B. Das, M. K. Das, and W. Weissflog, *Phase Transiions*, **82**, 433 (2009).

[29] A. Prasad and M. K. Das, *J. Phys.: Condens. Matter*, **22**, 195106 (2010).

[30] S. K. Sarkar and M. K. Das, *RSC Adv.*, **4**, 19861 (2014).

[31] M. F. Vuks, *Opt. Spectrosc.*, **20**, 361 (1966).

[32] S. Chandrasekhar and N. V. Madhusudana, *J. Phys.* (*Paris*), **30**, C4-24 (1969).

[33] H. E. J. Neugebauer, *Can. J. Phys.*, **32**, 1 (1954).

[34] A. Saupe and W. Maier, *Z. Naturforsch. A*, **16a**, 816 (1961).

[35] H. S. Subramhanyam and D. Krishnamurthi, *Mol. Cryst. Liq. Cryst.*, **22**, 239 (1973).

[36] I. Haller, *Prog. Solid State Chem.*, **10**, 103 (1975).

[37] W. H. de Jue, *Physical Properties of Liquid Crystalline Materials*, Gordon and Breach, London (1980).

[38] I. Chirtoc, M. Chirtoc, C. Glorieux, and J. Thoen, *Liq. Cryst.*, **31,** 229 (2004).

[39] S. Yildiz, H. Özbek, C. Glorieux, and J. Thoen, *Liq. Cryst.*, **34,** 611 (2007).

[40] S. Erkan, M. Çetinkaya, S. Yildiz, and H. Özbek, *Phys. Rev. E.*, **86**, 041705 (2012).

[41] W. Kuczynski, B. Zywucki, and J. Malecki, *Mol. Cryst. Liq. Cryst.*, **34,** 611 (2007).

[42] A. Prasad and M. K. Das, *Phys. Scr.*, **84**, 015603 (2011).

[43] P. Galatola and C. Oldano, *The Optics of Thermotropic Liquid Crystals*, S. Elston and R. Sambles (Eds.), Tailor and Francis, London (1998).

[44] F. C. Frank, *Disc. Faraday Soc.*, **25**, 19 (1958).

[45] C. W. Oseen, *Trans. Faraday Soc.*, **29**, 883 (1933).

[46] H. Zocher, *Trans. Faraday Soc.*, **29**, 945 (1933).

[47] S. Chandrasekhar, *Liquid Crystals*, Cambridge University Press, Cambridge (1992).

[48] M. Kleman, *Points, Lines and Walls*, Wiley, New York (1983).

[49] P. G. de Gennes and J. Prost, *The Physics of Liquid Crystals*, Oxford University Press, Oxford (1993).

[50] S. Singh, *Liquid Crystals Fundamentals*, World Scientific, Singapore (2002).

[51] V. Fréedericksz and V. Zolina, *Trans. Faraday Soc.*, **29**, 919 (1933).

[52] H. Gruler, T. J. Scheffer, and G. Meier, *Z. Naturforsch.*, **27a**, 966 (1972).

[53] H. Gruler and L. Cheung, *J. Appl. Phys.*, **46**, 5097 (1975).

[54] L. Pohl and U. Finkenzeller, *Liquid Crystals – Applications and Uses*, B. Bahadur (Ed.), **Vol. 1**, World Scientific, Singapore (1990).

[55] P. P. Karat and N. V. Madhusudana, *Mol. Cryst. Liq. Cryst.*, **40**, 239 (1977).

[56] H. P. Schad, G. Baur, and G. Meier, *J. Chem. Phys.*, **70**, 2770 (1979).

[57] M. J. Bradshaw and E. P. Raynes, *Mol. Cryst. Liq. Cryst.*, **72**, 35 (1981).

[58] H. P. Schad and M. A. Osman, *J. Chem. Phys.*, **75**, 880 (1981).

[59] F. Leenhouts and A. J. Dekker, *J. Chem. Phys.*, **74**, 1956 (1981).

[60] G. Czechowski and J. Jadżyn, *Acta Phys. Pol. A*, **106**, 475 (2004).

[61] T. Uchida and Y. Takahashi, *Mol. Cryst. Liq. Cryst.*, **72**, 133 (1981).

[62] P. Chattopadhayay and S. K. Roy, *Mol. Cryst. Liq. Cryst.*, **257**, 89 (1994).

[63] Y. Zhou and S. Sato, *Jpn. J. Appl. Phys.*, **36**, 4397 (1997).

[64] S. T. Wu and C. S. Wu, *Phys. Rev. A*, **42**, 2219 (1990).

[65] M. L. Dark, M. H. Moore, D. K. Shenoy, and R. Shashidhar, *Liq. Cryst.*, **33**, 67 (2006).

[66] M. K. Das and A. Prasad, *Mol. Cryst. Liq. Cryst.*, **540**, 162 (2011).

[67] P. Dasgupta, B. Das and M. K. Das, *Liq. Cryst.*, **39**, 1297 (2012).

[68] M. K. Das, A. Pramanik, B. Das, L. Szczucinski, and R. Dabrowski, *J. Phys. D: Appl. Phys.*, **45**, 415304 (2012).

[69] A. Pramanik, B. Das, M. K. Das, K. Garbat, S. Urban, and R. Dabrowski, *Liq. Cryst.*, **40**, 149 (2013).

[70] Hp. Schad, *J. Appl. Phys.*, **54**, 4994 (1983).

[71] P. Martinot-lagarde, *J Phys Lett.* (*Paris*), **38**, 17 (1977).

[72] K. Miyasato, S. Abe, H. Takezoe, A. Fukuda, and E. Kuze, *Jpn J Appl Phys.*, **22**, L661(1983).

[73] S. S. Bawa, A. M. Biradar, K. Saxena, and S. Chandra, *Rev Sci Instrum.*, **59**, 2023 (1988).

[74] A. Pramanik, M. K. Das, B. Das, M. Żurowska, and R. Dabrowski, *Liq. Cryst.*, **42**, 412 (2015).

[75] V. M. Vaksman, and Y. U. P. Panarin, *Mol. Mats.*, **1**, 147 (1992).

[76] L. M. Blinov and V. G. Chigrinov, *Electrooptic Effects in Liquid Crystal Materials*, Springer-Verlag, New York (1994).

[77] A. I. Allagulov, S. A. Pikin, and V. G. Chigrinov, *Liq. Cryst.*, **5**, 1099 (1989).

[78] J. F. Lyuu, C. C. Chen, and J. Y. Lee, *Mol. Cryst. Liq. Cryst.*, **329**, 99 (1999).

[79] A. K. Misra, A. K. Srivastava, J. P. Sukla, and R. Manohar, *Phys. Scr.*, **78**, 065602 (2008).

[80] W. Maier and A. Saupe, *Z. Natureforsch A*, **13a**, 564 (1958).

[81] W. Maier and A. Saupe, *Z. Natureforsch A*, **14a**, 882 (1959).

[82] W. Maier and A. Saupe, *Z. Natureforsch A*, **15a**, 287 (1960).

[83] R. L. Humphries, G. James, and G. R. Luckhurst, *J. Chem. Soc. Faraday Trans II*, **68**, 1031 (1972).

[84] W. L. McMillan, *Phys. Rev. A*, **4**, 1238 (1971).

[85] W. L. McMillan, *Phys. Rev. A*, **6**, 936 (1972).

[86] K. K. Kobayashi, *Phys. Lett. A*, **31**, 125 (1970).

[87] K. Kobayashi, *J. Phys. Soc. Jpn.*, **29**, 101 (1970).

[88] K. Kobayashi, *Mol. Cryst. Liq. Cryst.*, **13**, 137 (1971).